The HKU Scholars Hub   The University of Hong Kong   香港大學學術庫

Title	SERS-Enabled Lab-on-a-Chip Systems
Author(s)	Huang, J; Zhang, YL; Ding, H; Sun, HB
Citation	Advanced Optical Materials, 2015, v. 3 n. 5, p. 618-633
Issued Date	2015
URL	http://hdl.handle.net/10722/210725
Rights	This is the accepted version of the following article: Advanced Optical Materials, 2015, v. 3 n. 5, p. 618-633, which has been published in final form at http://onlinelibrary.wiley.com/doi/10.1002/adom.201400534/abstract;jsessionid=624C0ECFDB579D7FB9689BE071227426.f01t04

SERS-enabled Lab-on-a-Chip Systems

Jian-An Huang, Yong-Lai Zhang,* Hong Ding, and Hong-Bo Sun*

((Optional Dedication))

Dr. Y. L. Zhang, Prof. H. B. Sun
State Key Laboratory on Integrated Optoelectronics, College of Electronic Science and
Engineering, Jilin University, 2699 Qianjin Street, Changchun, 130012, People's Republic of
China.
E-mail: yonglaizhang@jlu.edu.cn; hbsun@jlu.edu.cn
Dr. J. A. Huang
Department of Electrical and Electronic Engineering, the University of Hong Kong, Hong
Kong SAR, China
Prof. H. Ding,
State Key Laboratory of Inorganic Synthesis and Preparative Chemistry, College of
Chemistry, Jilin University. Changchun, 130012, People's Republic of China.

ABSTRACT:

Surface-enhanced Raman spectroscopy (SERS) has been combined with microfluidic Lab-on-a-Chip (LoC) systems for sensitive optofluidic detection for more than a decade. However, most microfluidic SERS devices still suffer from analyte contamination and signal irreproducibility. In recent years, both the microfluidics and SERS communities have developed their own solutions that are complementary to each other; their combination even reveals the potential of commercialization. In this review, we summarize the recent advances in both fields for the development of reliable multifunctional SERS-enabled LoC systems and their broad applications. Starting from SERS fundamentals, we discuss reproducible SERS substrates and dynamic microfluidic trapping. Based on their combination, on-chip applications beyond SERS are presented, and insight can be gained into the commercialization of portable SERS chips.

1. Introduction

Microfluidic chips or lab-on-a-chip (LoC) systems, which could integrate entire laboratory processes within a nail-sized chip, have found broad applications, including chemical assays[1], biological detection[2], and chemical synthesis[3]. Microfluidic channels could confine and manipulate a solution, liquid, or suspension in a small micro-scale dimension so that distinctive small effects appear: for instance, the diffusion lengths of reagents are shortened, and the reaction could take place faster.[4] Accordingly, microfluidic devices exhibit many advantages compared with macroscopic instruments, such as low sample consumption, short reaction time, parallel analysis, and portability.[4-6] Meanwhile, a small sample volume requires highly sensitive detection techniques. The recent trend of on-chip detection methods in LoC systems employs optodetection techniques, because they can provide sensitive, rapid, clean and nondestructive monitoring functions.[7]

Among various on-chip optical detection techniques, surface-enhanced Raman spectroscopy (SERS) is emerging as a superior technique that features label-free fingerprint Raman spectra of reagents with narrow spectroscopic bands as well as ultrahigh sensitivity.[8, 9] The combination of the SERS technique with microfluidics started from the use of noble metal nanocolloids as flowing SERS substrates in microfluidic channels.[10] Aggregated nanocolloids could form interparticle gaps with spacings of less than 10 nm, known as nanogaps. Under excitation at the resonance wavelength, the nanogap could generate a significantly enhanced electromagnetic (EM) field, so-called "hot spot". If molecules happen to be excited at the hot spots, their emitted Raman signals would be enhanced by the EM field up to a single-molecule detection level.[11, 12]

Injecting SERS-active metal colloids into a microfluidic channel not only acts as an efficient monitoring platform for LoC systems but also benefits the improvement of SERS technology. Microfluidic flow could effectively dissipate heat and remove photo-damaged

analyte molecules from the detection volume under high-power laser excitation.[7] This benefits biomolecule detection, which typically requires high-power laser excitation and a long integration time for recognizable Raman spectra. In addition, the SERS signal reproducibility could be improved in microfluidic channels by averaging the collected signals from analytes that continuously flow through the detection volume.[10] However, SERS-active microfluidic devices based on metal colloids still suffer from poor SERS signal reproducibility due to the random colloid aggregation. For example, the Brownian motion of the colloids would result in a clear fluctuation of the SERS signals over time.[9] Furthermore, the laminar microfluids requires a complex channel design to fully mix the colloids with analytes, which adversely lead to cross contamination and channel clogging.[10, 13, 14] These drawbacks severely hinder their practical application.

In recent years, the rapid progress of nanotechnology has triggered significant advancements in reproducible SERS substrates as well as SERS-enabled LoC systems to address the aforementioned problems. Because SERS substrates are the foundation of microfluidic SERS detection, the solutions based on reproducible SERS substrates are particularly critical. Accordingly, SERS signal fluctuations could be suppressed by either regulating the EM field of individual metal colloids in single-particle SERS systems, or fabricating an ordered metal nanoparticle array with fixed nanogaps on solid-state substrates.[8] Cross-contamination and channel clogging could be avoided in microfluidic chips equipped with solid-state SERS substrates that will not flow with analytes.[15] On this basis, implanting solid-state SERS substrates within microfluidic devices could enable SERS-independent functions in SERS-enabled LoC systems, such as microfluidic chemical reactors.[16]

On the other hand, LoC systems could serve as an integrated platform to make SERS detection more reproducible, efficient, safe and environmentally friendly. For example, recent microfluidic reversible manipulation allowed for controllable colloid aggregation in

microfluidic channels.[17] More importantly, dynamic molecule trapping in microfluidic devices could address the uneven distribution of analytes (*e.g.*, the coffee-ring effect) on solid-state SERS substrates.[18] Furthermore, the flexible integration of SERS substrates with microfluidic chips would also contribute to the commercialization of portable SERS chips.

The combination of microfluidics with SERS not only provides new opportunities for both techniques as listed above, but also paves the way for multifunctional SERS-enabled LoC systems beyond SERS detection, which is often overlooked by both communities. In this review, we will bridge this gap by discussing the recent advancements in both SERS-enabled LoC systems and reproducible SERS substrates, as well as their complementary combination. For better understanding the fundamental role of SERS substrates in SERS-enabled LoC systems, the fundamentals of SERS will be briefly described in Section 2. Section 3 will discuss technical progress with respect to the fabrication of multifunctional SERS-enabled microfluidic devices, including reproducible SERS substrates and microfluidic dynamic trapping methods. Applications of SERS-enabled LoC systems in chemical and biological detections, as well as the commercial perspective of portable SERS devices, will be discussed in Section 4. Finally in Section 5, we will conclude with current challenges and offer a future outlook of multifunctional SERS-enabled LoC systems.

2. Fundamentals of SERS

The enhancement effect of SERS can be attributed to both electromagnetic enhancement (EME) and chemical enhancement (CE). The former originates from the strongly amplified EM field of the noble metal nanostructures with an enhancement range from 10^5 to 10^{10},[19] whereas the latter stems from the modification of Raman polarizability.[20-22] Because the optical power of Raman signals is proportional to the square of the molecule Raman

polarizability multiplied by the EM field at the molecule position, EME is generally 10^2-10^4 times stronger than CE and therefore accounts for the majority of SERS enhancement.[8, 12]

To understand the EME, special attention should be paid to the localized surface plasmon resonance (LSPR) of the metal nanostructures that leads to the enhanced EM field. Consider silver nanoparticles (AgNPs) as an example: LSPR could occur when the size of AgNPs is comparable to or smaller than the wavelength of the incident light. At a specific resonant frequency, the EM field of the incident light, E_0, induces collective oscillation of the AgNP conduction electrons, which is a phenomenon called LSPR. As a result, the optical energy of the incident light is coupled steadily to those of the EM field of the oscillating electrons.[23] Therefore, AgNPs act as optical antennas to condense optical energy on their surface through LSPR. Thus the magnitude of the EM field, E, is significantly enhanced and exponentially decays away from the AgNP surfaces. The spatially confined field then excites the molecules adsorbed on the AgNP surfaces to emit enhanced Raman signals. As the emitted signals pass the EM field again before arriving at detectors, they are enhanced twice by the EM field at both the excitation and emission steps. Because the far-field radiated power of Raman signals is proportional to the square of the EM field, the EME could be approximated as in the scale of $|E/E_0|^4$ if the wavelength difference between the incident light and Raman band could be ignored. [9, 24, 25]

Moreover, the EM field in the nanogap between two neighboring AgNPs can be further enhanced by as high as 10^8 when the AgNP LSPR is coupled with one another (Figure 1a).[19] The LSPR coupling depends on the nanogap spacing and laser polarization. A polarization-dependent SERS experiment indicated that the LSPR coupling in an AgNP dimer led to the highest field enhancement when the incident excitation polarization is parallel to the nanoparticle axis (Figures 1b and 1c). However the enhancement reduced to a minimum at perpendicular polarization. The field enhancement of LSPR coupling of the AgNP dimer at

parallel polarization could be understood qualitatively through molecule orbitals. When two atoms approach each other and form a molecule, the electron clouds of their outer orbital start to interact with each other. They eventually form a molecular bonding state with lower overall energy and an antibonding state with higher energy. The bonding state exhibits high electron density in the middle between the two atoms such that the Coulomb repulsion is better screened between the nuclei, leading to lower overall energy. Similarly, the EM field of the coupled LSPR in an AgNP dimer would reach a stable "bonding" state with high EM energy accumulated in the nanogap and lead to the ultrahigh field enhancement. The polarization dependence of LSPR coupling in SERS is important in the research of single-molecule detection, in which the molecule orientation and surface selection rules in the nanogaps are studied by SERS spectra. However, it could induce non-uniform EM fields in the nanogaps of the AgNP clusters, where the dimer axes are not all parallel to the incident polarization.

Whereas EME is a universal effect, CE in SERS would be evident only for suitable analyte molecules, because it depends on the Raman polarizability modification of molecules bonding to the metal surface. To understand CE, one should consider that the magnitude of Raman polarizability depends on the available optical transitions. According to the popular charge transfer (CT) mechanism, CE is possible when the Fermi level of metal is in between the energy levels of the highest occupied molecular orbital (HOMO) and the lowest unoccupied molecular orbital (LUMO) of the adsorbed molecules. When the molecules form covalent bonds with the metal surface, photo-induced transitions of electrons occur either between the adsorbate HOMO and the vacant states of metal above the Fermi level, or between the occupied states in metal below Fermi level and the adsorbate LUMO, under an optical excitation of a wavelength matching the transition energy. In view of the CT process, CE is similar to resonant Raman scattering (RRS), in which enhancement is obtained when an electronic transition of probed molecules is close in wavelength to the excitation light.[26-28] By

the similar enhancement mechanism of SERS, surface-enhanced resonant Raman scattering (SERRS) with chromophore labeling and a wavelength-tunable laser exhibits narrower and more sensitive Raman peaks against fluorescence, emerging as a promising multiplexing detection tool in biological analysis.[29, 30]

To experimentally evaluate the enhancement capability of an SERS substrate, the enhancement factor (EF), defined as the Raman enhancement per unit molecule by the SERS substrate with respect to the normal Raman signals, can be calculated by the following formula:

$$EF = \frac{I_{SERS} / N_{SERS}}{I_{RS} / N_{RS}} \tag{1}$$

where I_{SERS} is the Raman intensity of a specific Raman band of the molecules absorbed on and enhanced by the SERS substrate, N_{SERS} is the number of molecules absorbed on the SERS substrate, I_{RS} is the normal Raman intensity of the same Raman band of the molecules under normal Raman measurement, and N_{RS} is the number of molecules under normal Raman measurement. The geometry of the SERS substrate and the detection volume of the objective of the Raman spectrometer for molecule counting are typically considered in the calculations.[9, 31]

To evaluate the sensitivity of the SERS substrate, another application-oriented parameter called limit of detection (LoD) is used, which is the lowest analyte concentration required to achieve a signal that is three times stronger than the background noise.[32] Whereas EF attempts to remove the influence of the Raman instrument and focuses on the SERS substrates, LoD is related to the sensitivity of the Raman spectrometer, the SERS substrate and the analyte molecules. For example, a longer integration time might lower the LoD but not the EF because both SERS and normal Raman measurements are conducted under the same

integration time. An SERS substrate with a high EF should lead to a lower LoD, but the inverse is not necessarily the case.

3. Fabrication of multifunctional SERS microfluidic chips

There are two categories of SERS substrates that could be integrated in microfluidic devices for SERS detection: metal colloids and solid-state substrates.[8, 33] The former is beneficial due to ease of use, because the pre-synthesized metal colloids could be directly injected into microfluidic channels for subsequent SERS detection. In addition, colloid-based SERS microfluidic cells can provide controllable flow conditions, which would average the signal variations, decrease the local heating and thus improve the detection limit.[10, 34-36] However, the use of metal colloids inside a microfluidic chip causes new problems, such as a long mixing time, difficulties in sample separation and even channel clogging. These problems could be avoided in the case of solid-state SERS substrates, which would not flow with analytes. Moreover, to generate uniform "hot-spot" arrays, solid-state SERS substrates allow for precise control over the nanogap distance, which is essential for obtaining an enhanced EM field and high reproducibility. A recent trend of on-chip SERS detection typically resorts to the integration of solid-state SERS substrates.[13, 37]

3.1 Reproducible metal colloids for SERS-active microfluidic chips

Ag colloid suspension was the first SERS system that was introduced into microfluidic devices due to its simple synthesis procedure.[38, 39] The synthesis of Ag colloids relied on charged surfactants as stabilizing and separating agents, but the surface charge may lead to problems in generating reliable SERS signals. For example, the ionic environment changes would induce colloid aggregation, which could generate an EM field significantly stronger than the single colloid. Together with the random aggregation due to the Brownian motion,

the large difference in the EM fields between single colloids and colloid aggregates resulted in the signal irreproducibility of metal-colloid-based SERS-active microfluidic chips. Moreover, the colloid surface charge can prevent the adsorption of molecules with the same charge. Therefore, the number of molecules adsorbed on the colloid surfaces was difficult to estimate, and thus, the SERS EFs of colloids in many cases were evaluated by $|E/E_0|^4$.[9]

Single-particle SERS (spSERS) substrates have been developed as reproducible SERS colloids for microfluidics to generate an EM field of individual colloids similar to that of colloid aggregates. Typical examples were silica-Ag core-shell nanoparticles that could tune the EM field by varying the particle size and shell thickness (Figure 2a).[40-46] As spSERS substrates, single core-shell nanoparticles exhibited EME on their surfaces comparable to that in the nanogaps of AgNP dimers. The enhanced EM field originated from the coupling of LSPR of their inner and outer interfaces. On the other hand, shaped metal nanoparticles, such as gold (Au) nanostars, would exhibit a strong EM field at the sharp corners comparable to nanogap fields (Figure 2b).[47-50] With an EM field that can be tuned by the particle geometry, the single Au nanostar exhibited a SERS EF as high as 10^7, approaching the EF in nanogaps.[49] In addition, the Tian group[51-58] invented shell-isolated nanoparticle-enhanced Raman spectroscopy (SHINERS) utilizing Au-silica core-shell nanoparticles with a controlled silica shell thickness for maximum Raman enhancement (Figure 2c-e). The silica shell was well controlled to prevent the nanoparticles LSPR from coupling with each other. As a result, no dimer nanogaps existed, and thus, single nanoparticles shared the same EM field as the nanoparticle clusters. To summarize, spSERS colloids indicated that a single colloid exhibited EME in similar manner as the colloid cluster. Therefore, when they were mixed with analytes in microfluidic devices, their random aggregation would induce only slight variations in the Raman signals, and the signal reproducibility could be effectively improved.

3.2 Controllable colloid aggregation in microfluidic channels

Whereas spSERS colloids could improve signal reproducibility based on advanced synthesis methods, reversible microfluidic trapping not only allowed conventional metal colloids to form aggregates on demand, but also helped to solve the clogging problem. Recently, Kim et al.[13] developed a bias-mediated trapping/releasing method for the controllable *in situ* aggregation of colloids in the detection volume. Conductive polymer electrodes were fabricated on both sides of a microfluidic channel. The electrodes under bias could repel Au colloids with a negative surface charge such that Au nanocolloids were trapped or released under different biases (Figure 2f). However, the electrodes might also attract analytes with positive charges and risk losing analytes. As a more universal dynamic trapping, Zhou et al.[59] integrated two PDMS pneumatic valves and nanopost array into the bottom of a T-shaped microfluidic chip. In their work, a mixture of Au colloids and analytes could be effectively trapped by the nanopost array because the channel could be reversibly narrowed by the pneumatic valves under external pressure. After SERS detection, the channel could be widened by the valve, and the colloids and analytes were released. Although the LoD of this device could reach the picomolar level, the channel narrowing inevitably affected the flow rate, making the SERS signal unstable. A better reversible optoelectrofluidic trapping of colloid clusters was developed by Hwang et al.[60], who coated a photoconductive layer on a liquid chamber for the SERS measurement of a mixed solution of Rhodamine 6G (R6G) and Au nanoparticles. By applying an alternating current (AC) electric field between the photoconductive layer and ground electrode, the laser-illuminated area of the photoconductive layer exerted a non-uniform electric field on the liquid. As a result, Au nanoparticles aggregated within the laser detection volume and formed SERS hot spots. The device appeared promising to generate reproducible and sensitive microfluidic SERS signals, because the aggregation control was accurate and no negative effect was introduced.

Both spSERS nanoparticles and on-chip reversible trapping of colloid clusters aimed to improve the signal reproducibility for the metal-colloid-based SERS chips. However, in both cases, metal colloids had to be mixed with analytes for SERS detection, which inevitably contaminated the analytes and affected the post-SERS processes. In this regard, the development of solid-state SERS substrates becomes crucial.

3.3 Emerging solid-state SERS substrates for microfluidic chips

Solid-state SERS substrates are typically made by depositing order metal nanoparticle arrays with fixed nanogaps on planar substrates. The nanogaps could be tailored to generate similar intense EM fields in all nanogaps to achieve uniform EME. In contrast with metal colloids suspension, analytes adsorb on solid-state SERS substrates in the dry state, and therefore, the signal fluctuation over time due to dynamic colloid motion is avoided. When the solid-state SERS substrates are embedded in microfluidic channels, they would not flow with analytes and thus allowed for SERS-independent analyte processing. In this case, the uniformity of either nanogap spacing or molecule adsorption becomes the main parameters affecting the SERS signals. The reproducibility of the SERS signal could be evaluated by the relative standard deviation (RSD, defined as the standard deviation divided by the mean) of the SERS spectra from spot to spot. Generally, high reproducibility corresponds to a low RSD, and SERS substrates with an RSD of less than 20% were typically accepted as reproducible.[61]

Although focused ion beam (FIB) and electron beam lithography (EBL) allowed for precise control over the nanogap spacing of metallic nanostructures, they were expensive and only allowed small regions to be fabricated, which limits their practical applications.[62, 63] In this regard, the cost-effective and large-area fabrication of well-controlled hot spots is highly desired. As pioneers, Van Duyne's group[64-66] adopted nanosphere lithography (NSL) to fabricate Ag film on nanospheres (AgFON) and Ag nanotriangle arrays. As shown in Figure

3, AgFON was formed by depositing a 120-nm-thick Ag layer on the hexagonal-close-pack polystyrene (PS) nanosphere monolayer on a glass slide, and Ag nanotriangles were left when the PS nanospheres were removed. Strong EM fields of coupled LSPR appeared in the nanogaps that were formed by either the tips of nanotriangles or the adjacent AgFONs. By changing the size of the nanosphere and the Ag layer thickness, the LSPR of Ag nanotriangles and AgFON could be tuned to match the excitation laser and achieve the maximum SERS EFs of 10^8 and 10^{11}, respectively.[8] An LoD as low as 1.5 ppb in detecting airborne species has also been achieved *via* NSL.[67, 68] The ordered nanospheres array directly led to the high signal reproducibility of AgFON with an RSD as low as 6.5%.[69, 70] Therefore, NSL offered a flexible, low-cost and wafer-scale fabrication method that could make ordered nanoarrays with accuracies comparable to those of EBL and FIB.[71]

Based on NSL, Au nanovoids (the inversion of metal nanodot arrays) have been developed as a reproducible SERS substrate by the electrochemical deposition of Au on the nanosphere monolayer followed by the dissolving of nanospheres.[72] In comparison to Ag nanotriangle arrays, an individual spherical nanovoid could confine greater energy of the EM field and thus acted as a highly sensitive SERS hot spot. Ordered Au nanovoids also facilitated the uniform molecule adsorption. As a result, a SERS EF of 3×10^6 and an RSD of less than 10% were obtained for an area of approximately 0.5 cm^2.[24] Additionally, the plasmonic behavior of Au nanovoids could be engineered by changing the Au layer thickness and nanovoid diameters.[73] Recently, He *et al.*[74] grew Ag nanosheets on the framework of a Au nanovoid array to combine the nanovoids with nanogaps formed between standing Ag nanosheets as the hot spots. The SERS EF was increased by one order of magnitude to 6×10^7, and highly sensitive on-chip detection of R6G (10 fM) and label-free DNA (5 nM) were demonstrated.

Another promising SERS substrate based on modified NSL was the nanocrescent arrays that were fabricated by tilted thin-film deposition and subsequent ion milling of the nanosphere template on glass.[75-78] Nanocrescents exhibited different LSPRs at the tips or bodies at different wavelengths depending on the polarization direction of the excitation. Consequently, an EF as high as 10^{10} was achieved in the measurement of R6G.[78] Moreover, Wu et al.[79] fabricated crescent-shaped nanoholes through a similar procedure. The nanoholes featured sub-10-nm gaps at both tips, which were sharper than those of the corresponding nanocrescents. The coupled LSPR yielded an EME of up to 10^{12}. Recently, Lipomi et al.[80] used nanoskiving to transfer Au nanocrescents on the cleaved facets of an optical fiber, which might be broadly applied in portable SERS detection as well as microfluidic chips.

To further enhance the precision of nanogaps, atomic layer deposition (ALD) was adopted to make sub-10-nm metallic nanogaps for sensitive and reproducible SERS substrates. As reported by Im et al.[81, 82] a thin layer of alumina oxide coated by ALD was used as sacrificial layer to fabricate sub-10-nm Ag nanogaps. Compared to the NSL and EBL methods, the nanogaps prepared in this method could be well controlled by tuning the thickness of the alumina layer in the range of 5-20 nm over the large area. The SERS EF reached 10^9 at the nanogaps with a 5 nm spacing on 90% of the wafer area.[82]

In addition to the ordered nanogap arrays, uniform molecule adsorption was another important factor that affected the signal reproducibility. Fang et al.[83] experimentally demonstrated that the non-uniform molecule adsorption was the origin of SERS irreproducibility. As illustrated in Figure 1, the highest EF of 10^8 appeared in the narrowest gap, which allowed for the absorption of only a small number of molecules. In contrast, most molecules were located on the open surface area of the particle where the EF was less than 10^5.[83] Therefore, efforts have been made to develop nanowire-based SERS substrates that could form nanogaps after the adsorption of molecules.[84-87] Figure 4c shows flexible Au-

coated polymer nanofingers fabricated by nanoimprint lithography. During the evaporation of solvents, the capillary force would drive the nanofinger aggregation and thus form nanogaps between adsorbed molecules.[86] The polymer offering flexible nanofinger aggregation also presented Raman bands that contaminated the analyte spectra. To avoid the influence of Raman bands from polymers, Schmidt *et al.*[87] developed Ag-coated silicon nanopillar array by reactive ion etching and metal deposition. After the molecule adsorption and capillary-force-driven aggregation, the silicon nanopillars exhibited a maximum SERS EF of 2.1×10^{11} and an RSD of 8% for an area of 10×10 cm^2. Another way to average the signal difference from non-uniformly adsorbed molecules was to increase the amount of SERS hot spots. Accordingly, a metal nanoparticle coated on nanowire arrays could accommodate more metal nanoparticles than planar substrates and thus generate more hot spots.[18, 88-93] As a typical example, Oh et al.[89] coated Ag nanoislands on glass nanopillar arrays to create dense hot spots on the top and sidewall of the nanopillars (Figures 4a and 4b). In their work, a SERS EF over 10^7 with a low RSD of 7.8% was achieved. In addition, Xu et al.[88] coated AgNPs on ordered silicon nanocone arrays for the SERS detection of label-free DNA at 10^{-8} M. Such a low LoD and high signal reproducibility could be attributed to the significantly increased SERS hot spots in the hierarchical SERS substrates.[89, 94, 95]

A thorough method to overcome the non-uniform molecule adsorption in nanogaps was to replace nanogaps by open enhancing surfaces.[40, 96] Open surfaces allowed for easy and uniform molecule adsorption. Although the EM field of open surfaces without LSPR coupling would be lower in intensity, it spread widely to cover as much adsorbed molecules as possible to increase the amount of collected signals. Furthermore, the EM field of LSPR on an open surface should be uniformly distributed such that the covered molecules are equally excited. Accordingly, Huang *et al.*[97] fabricated Ag-coated, ordered silicon nanowire (Ag/SiNW) arrays with a designed Ag thickness, wire diameter and length. As shown in Figure 4d, the

nanowires were separated by 150 nm, and the Ag layers of the Ag/SiNWs were continuous. As a result, each nanowire behaved as a waveguide of the propagating surface plasmons that could propagate along the nanowire and spread its EM field widely over the entire wire surface. Benefitting from the wide-range field, the Ag/SiNW substrate was able to detect double-strand DNA of 25-50 nm in length with a low RSD of 14% for measurements of more than 4,000 spots. Quantitative analyses of multiplexed SERS detections have also been demonstrated with an EF of 10^6, an RSD of 7% and a correlation coefficient of 0.978.[98]

To provide an overview of the solid-state SERS substrates reported to date, we have summarized the recent advancements in Table 1. The typical nanostructures, fabrication methods, SERS enhancement and signal reproducibility of these solid-state SERS substrates are presented as a guide for researchers who might consider embedding one of these substrates into their microfluidic chips. The solid-state SERS substrates would not contaminate analytes and could hold great promise for reproducible and multifunctional on-chip SERS detection, because the rapid progress of the chip fabrication techniques allows for the integration of various multifuctional components in microfluidic devices.[16]

3.4 Integration of solid-state SERS substrates with microfluidic devices

Together with analyte contamination, the integration of solid-state SERS substrates in microfluidic chips could address many other problems, such as the long mixing time, clogging, and loss of analytes.[13] Embedded solid-state SERS substrates in microfluidic SERS chips would exhibit higher signal reliability due to the absence of dynamic colloid motions as discussed previously.

Currently, the integration of solid-state SERS substrates with microfluidic devices could be realized in two ways. One is the *in-situ* fabrication of SERS-active metallic micronanostructures inside a microfluidic channel, and the other is the construction of

microfluidic channels on top of the SERS substrates. For the former route, one convenient way is to immobilize metal nanoparticles in microfluidic channels. Takahashi et al.[99] reported the integration of a 3D Au photonic crystal (PC) structure through the co-assembly of Au colloidal nanoparticles and large PS nanospheres inside a microfluidic channel. After the removal of the PS nanospheres, the Au SERS structure exhibited an LoD of 1 nM in the flow measurement of a 4,4'-bipyridine solution. In addition, the *in-situ* chemical synthesis of SERS structures inside a microfluidic channel effectively exploited the microfluidic technology. Parisi et al.[100, 101] reported the *in-situ* synthesis of Ag NPs on the sidewall of the channel through chemical reactions between Ag^+ and electrodeposited Cu. Similarly, Leem et al.[102] fabricated a nanostructured Ag film on the bottom and sidewall of the channel by heat treatment of Ag precursor.

In addition to the chemical routes, another cleaner and more convenient way to integrate a metal nanostructure in a microfluidic channel is laser micronanofabrication, which could realize SERS-active microfluidic devices in a designed manner.[103-106] The femtosecond laser direct writing (FsLDW) technique is recognized as a powerful nanofabrication tool that could fabricate 3-dimensional complex nanostructures on a wide range of materials.[16, 107] Using FsLDW, Xu et al.[106] reported the fabrication of highly sensitive Ag SERS substrates within a glass microfluidic channel through the laser-induced photoreduction of the Ag^+ precursor. The resultant Ag structures are constructed by crystallized Ag nanoplates of different shapes and thicknesses, and the SERS monitor could be precisely located at any required spot in the channel to achieve a maximum SERS EF of approximately 10^8. The researchers subsequently used the FsLDW technique to fabricate a Ag microflower array directly in a microfluidic channel for a catalytic reaction.[104] Figure 5a shows the basic concept of their works. The resultant Ag microflowers were composed of upright Ag nanoplates with nanoparticles on each plate surface (Figure 5b-d). The hierarchical structures contribute to their considerable

roughness, giving rise to significantly enhanced SERS signals. Interestingly, the Ag microflower could act as both a catalytic active site and an *in-situ* SERS monitor for a given chemical reaction.

Alternatively, SERS substrate-embedded microfluidic devices could be fabricated by covering a pre-patterned micro-channel system on flat solid-state SERS substrates. For example, Lai et al.[108] annealed a Ag film to Ag NPs on a silica substrate before embedding it in a channel, and Oh and Jeong[109] fabricated SERS-active nanopores by oxygen plasma etching of the Ag film deposited on the bottom of a microfluidic chip. Moreover, Xu et al.[110] used two-beam femtosecond laser interference to fabricate grating structures with tunable periods on a photoresist layer and coated the surface with a Ag nanolayer as SERS substrates. Finally, a PDMS channel prepared by soft lithography was covered on the substrate to achieve a SERS-active microfluidic device. In addition, Vlasko-Vlasov et al.[111] used FIB to fabricate eight concentric nanoslits on a Ag film that was coated on a glass slide as microscopic plasmon lenses. A cover glass slide with two holes for the fluidic inlet/outlet and an etched central part as a channel was covered on the bottom slide to form a SERS microfluidic chip.

3.5 Dynamic trapping of the analyte in SERS-active microfluidic chips

The fluid in the microfluidic channel is laminar flow, so only part of the fluid in the channel flows through the EM field of the embedded SERS-active sites. In this regard, analytes trapping over the embedded solid-state SERS structures in the microfluidic system becomes a crucial issue. One successful example was reported by Oh et al.[112] who trapped molecules by points of zero velocity, called "stagnation points", near SERS hot spots in AgFON nanofluidic channels. The authors demonstrated that the probability of the R6G molecules being trapped in the hot spots increased by one order of magnitude compared to bare AgFONs film, and the SERS EF was 10-fold higher.

In addition, embedded solid-state SERS microfluidic devices also allow dielectrophoresis (DEP) manipulation for reversible on-chip molecular trapping.[113] DEP is an electrostatic attractive or repulsive effect of small objects that occurs in inhomogeneous electric fields. Sharp metal tips would have a higher electric field gradient under AC bias and thus exhibit a higher DEP force. As a result, the DEP force could attract molecules on the tip surface under the bias of the molecules' crossover frequencies and release them when the bias was turned off. For example, a Au microwire array was embedded in a microfluidic channel as an efficient DEP-based SERS microfluidic chip that could immobilize bacteria from blood.[114] Similarly, a rough Au surface in a DEP-based SERS-active microfluidic device was developed to separate bacteria and red blood cells from a blood sample and concentrate them in different microfluidic channels by applying biases with different crossover frequencies. Then, the separated bacteria were trapped on a rough Au surface for subsequent SERS detection.[37, 115]

Recently, an SERS-active nanowire array that exhibits a large surface area was successfully embedded in LoC devices for dynamic analyte trapping.[15, 116-119] As a typical example, Perozziello et al.[119] demonstrated a 3-way microfluidic trapping of cells by embedding Au nanoneedles as both cell trapping and SERS detectors in a microfluidic device. In their work, the Au nanoneedles were fabricated by EBL on a joint point of a 3-way channel that had inlet/outlet holes and a microfluidic layout. As shown in Figure 6, a cell could be located on the SERS-active Au nanoneedles by controlling the flow directions of the 3 microfluidic channels. The 3-way channels could even change the orientation of the cell for the SERS analysis of different spots of the cell membrane.

The work of Perozziello et al. served as an excellent prototype of a multifunctional SERS-enabled LoC system because it demonstrated the SERS-independent microfluidic manipulation of cell orientation as well as a SERS analysis of the cell membrane. SERS-

active Au nanoneedles acted as a detection room in a laboratory to which the analytes were delivered once again after other processes (cell rotation). In this regard, solid-state SERS detection sites allowed for contamination-free analyte processing in other steps, and dynamic analyte trapping helped to locate analytes at specific functional microfluidic sections. These two features already laid the foundation for SERS-enabled LoC systems as a universal microfluidic laboratory platforms.

4. Applications of SERS-enabled LoC systems

New technologies could lead to new applications. SERS-enabled LoC devices combining dynamic microfluidic trapping and reproducible SERS substrates provided an integrated platform for reliable optofluidic detection, such as biomolecule identification, immunoassay, reaction monitoring, and biomolecular surface binding. Moreover, the integration of solid-state SERS substrates would trigger additional applications beyond SERS detection, such as catalytic active sites, analyte manipulation units, and conductive electrodes.

4.1 Analysis of deoxyribonucleic acid (DNA) and ribonucleic acid (RNA)

The analysis of DNA and RNA sequences is important in molecular biology and diagnosis, because the characterization of particular diseases is often dependent on the nucleic acid identification. Compared to conventional fluorescence techniques, the non-invasive SERS detection of DNA and RNA featured label-free and multiplexing due to the sensitive fingerprint Raman spectra with narrow bands.[30] Recently, a microfluidic DNA chip was developed by immobilizing capturing DNA on the bottom of the microfluidic channel via a rapid automated process.[120] After injecting a DNA solution with AgNPs, the SERS signals of the target DNA were detected only on the spots with immobilized complementary DNA that could be hybridized with the target DNA. Choi et al.[121] further developed a programmable

AgNP-based gradient microfluidic SERS device for the simultaneous detection of two different DNA in their mixtures through quantitative analysis. The microfluidic channels network in the device was designed to generate different concentrations of the injected mixture. Therefore, the SERS signals of the two DNA in different ratios of DNA mixtures could be measured in flow conditions and distinguished by quantitative analysis within 10 min. Furthermore, to avoid the problems of AgNP clogging and the memory effect, Prado et al.[122] produced droplets hosting Ag colloids and RNA analytes in a microfluidic platform (Figure 7a). The mixture of analytes and colloids aggregation would be confined in the droplets. As a result, the reaction time could be reduced, and colloid contact with channel sidewalls could be minimized. As shown in Figure 7b, the bell-shaped SERS intensity distribution of a polycytosine Raman band indicated that the analytes were well confined in the droplet. Meanwhile, the evolution of a polycytosine SERS profile with mixing time in Figure 7c and 7d demonstrated that no colloid aggregation was detected on the channel sidewall. The work demonstrated that the combination of droplets with metal colloids in microfluidic devices could be a promising low-cost approach for label-free RNA detection.

4.2 Study of biomolecular surface binding

The surface binding of biomolecules in aqueous media is an important issue in many fields, such as drug delivery. Recently, aptamers have been applied in SERS-active microfluidic systems to study binding events. Aptamers are short single-stranded oligonucleotides of DNA that can react with many target molecules, such as proteins, drugs, and toxins. Thiolated aptamers can form robust sulfur-metal bonds on Au or Ag surfaces such that they serve to bind the analytes in the vicinity of the enhancing metal nanostructures for SERS detections. As a typical example, Banerjee et al.[123] covered an etched PDMS channel on an anodic alumina oxide (AAO) layer of an aluminum foil to form a SERS microfluidic

chip for monitoring protein binding to lipid bilayers. As shown in Figures 8a and 8b, the Raman spectra indicated that the streptavidin or zwitterionic phospholipid 1,2-dimyristoyl-sn-glycero-3-phosphocholine (DMPC) injected into the AAO microfluidic chip could be easily washed away. In contrast, the biotinylated DMPC could bind to the AAO surface such that the streptavidin bonded to their other ends could be detected after washing with water. By adding a mixed solution with a large suspended cell, *Salmonella enterica*, the authors further demonstrated that the proteins bound to the AAO surface by biotinylated DMPC were not affected by foreign cells (Figure 8d). In addition, Galarreta et al.[124] embedded nanotriangle arrays into a microfluidic chip for the SERS spectroscopic analysis of aptamer- ochratoxin-A (OTA) binding structures. The chip could identify the Raman spectra of OTA and the G-quadruplex conformation of the aptamer-OTA binding structure, showing high potential in the field of molecular structure recognition. Yun Suk and Erickson [125] used a nanotube-embedded PDMS microfluidic chip to detect Vasopressin (VP) with aptamers. A linear response of SERS intensity to VP concentration was obtained with a low detection limit of 5.2 µU/mL.

4.3 On-chip sorting and identification of bacteria

Reversible on-chip molecular trapping in solid-state SERS-enabled microfluidic devices was particularly useful in bacteria sorting, concentration and identification.[113] Recently, the separation and Raman detection of *S. aureus* from blood cells have been demonstrated in a Au-microwire-embedded microfluidic cell within 15 s after sample loading.[114] The high gradient of the electric field at the tips of microwires under an applied voltage increased the DEP mobility of the bacteria and the sorting speed. Similarly, Cheng et al.[37] fabricated a rough Au surface on a glass slide with patterned electrodes and then covered it by a top glass slide to form a SERS-active DEP microfluidic chip. Under the applied voltage of specific crossover frequencies, bacteria in a low-concentration solution were concentrated in the SERS

substrate within minutes due to the negative DEP force. The device successfully separated Gram-positive bacteria, *S. aureus*, from red blood cells and detected them with SERS technique. As shown in Figure 9, a mixture of 10^6 CFU/ml bacteria and a dilute blood sample were separated under an AC voltage with a frequency of 500 kHz and a flow rate of 1 ml/min. Because the bacteria experienced lower negative DEP mobility and the blood cells experienced a higher negative DEP mobility, bacteria and blood cells were concentrated at the lower subchannel and middle subchannel, respectively. The chip exhibited sorting efficiencies of 80% and 99% for *S. aureus* and blood cells, respectively. Recently, the same group fabricated a rough Au surface in the center electrode of a concentric round microfluidic device.[115] Under applied voltage, the device exhibited DEP, electrophoresis and electrohydrodynamics manipulation simultaneously, which contributes to the rapid separation, concentration, and *in-situ* SERS detection of three types of bacteria (*S. aureus, E. coli*, and *P. aeruginosa*) from human blood.

4.4 *In-situ* monitoring of chemical reactions

The unique features of microfluidics continuously stimulate the research interests of different disciplines. As an efficient experimental platform for catalytic reactions, a well-designed microfluidic device allows the reactants to achieve full contact with the catalytic active sites in a confined space, making the on-chip catalysis an interesting topic.[3] In addition, because Au and Ag are general catalytic-active materials, solid-state SERS substrates embedded in microfluidic channels could act as both catalytic active sites and SERS reporters. Recently, Xu et al.[104, 106] used a Ag microflower-embedded microfluidic channel as a microreactor for the reduction of 4-nitrophenol to 4-aminophenol. *In-situ* SERS monitoring of the reaction was realized simultaneously by using the same Ag microflower arrays as the SERS substrate. In their work, obvious SERS signals could be clearly detected after the

reaction for 2 min, and the conversion of 4-nitrophenol could reach nearly 100% within 7 min. Similarly, Paquet-Mercier et al.[126] embedded a plasma-etched metal thin film in a microfluidic chip as a bioreactor that could induce sheath flow confinement of a biofilm precursor stream. The chip enabled the *in-situ* SERS monitoring of biofilm flowing dynamics and growth on the channel sidewall. The integration of solid-state SERS substrates with microfluidic devices may find broad application in monitoring various *in-situ* processes.

4.5 Portable SERS-active LoC systems

To achieve the portability of microfluidic SERS detection systems, the recent miniaturization of SERS-enabled LoC systems focused on the integration of optical fibers to guide the laser into the chips and the Raman signals out of the chips.[34] As shown in Figures 10a-c, Yazdi et al.[127] designed a PDMS optofluidic chip that could trap the nanoparticles/analytes into a channel end for excitation and signal collection by integrated optical fibers. In their device, AgNPs and analytes were passively mixed in a 5-cm-long micromixer, and thiolated silica microspheres were added to bind the nanoparticles/analytes to their surface. When silica microspheres are trapped at the narrow channel for Raman detection, the detection limits of two food contaminants, melamine and thiram, could reach 63 ppb and 50 ppt, respectively. Meanwhile, metal-coated optical fibers have also been used for on-chip SERS detection. Fan et al.[128] used 3-aminopropyltrimethoxysilane to bind a AgNP monolayer to a cleaved optical fiber facet and demonstrated an in-line multiplex SERS analysis of 5 analytes in an aqueous solution with an LoD below 1 nM. Yap et al.[129] deposited a monolayer of Au nanoparticles on an optical fiber facet to demonstrate the SERS detection of crystal violet with an EF of $>10^7$.

In addition to the integration of SERS substrates with optical fibers, portable diode lasers and Raman spectrometers have also been used with SERS chips for on-site analysis. As

shown in Figure 10d, Kim et al.[130] fabricated SERS-active nanofinger arrays on a coin-sized chip that could be inserted into the sample slit of a palm-sized Raman spectrometer for on-site SERS detection. The highly sensitive detection of melamine in milk products has been achieved, in which the detection limits reached 120 ppt in water and 100 ppb in infant formula, respectively. The inserted SERS substrates and coupled palm-sized Raman spectrometer are critical to the development of portable on-chip SERS detection devices. With the rapid progress of the SERS technique, some low-cost and sensitive SERS substrates have been readily prepared using simple methods. For instance, some paper-based SERS substrates, so-called SERS test strips, have been prepared using general papers or biomaterials such as rose petals.[131-140] If SERS test strips could provide reliable and reproducible SERS signals, their integration with palm-sized Raman spectrometers would trigger the rapid development of portable microfluidic SERS detection systems.

5. Conclusions and Outlook

In conclusion, recent advancements in reproducible SERS substrates and dynamic microfluidic trapping have been reviewed to frame the development of multifunctional SERS-enabled LoC systems. First, a prerequisite was to obtain reproducible SERS signals in microfluidic channels. Single-particle SERS colloids that could generate similar EM fields as in colloid clusters were first introduced to overcome the signal variation due to random aggregation. Microfluidic techniques of controllable colloid aggregation for reproducible SERS signals were applicable to conventional Ag colloids and also received considerable attention. Aiming to generate similar EM fields in all fixed nanogaps, solid-state SERS substrates integrated in microfluidic channels not only served as reproducible SERS-active sites but also addressed the analyte contamination problem because they would not flow with analytes. Furthermore, dynamic microfluidic trapping allowed for the trapping of analytes on

SERS-active sites on demand, solving the issue of insufficient analytes adoption on solid-state SERS substrates in laminar microfluids. Therefore, embedded solid-state SERS substrates allowed for reproducible contamination-free analyte detection and post-SERS processing, and dynamic microfluidic trapping could deliver analytes to designated microfluidic sections. The combination of these techniques already set the foundation of multifunctional SERS-enabled microfluidic chips and their applications beyond SERS detection were also reviewed.

Currently, there are two major challenges for the development of a multifunctional SERS-enabled LoC system. The first challenge is the integration of solid-state SERS substrates in microfluidic chips. Current microfluidic channels equipped with solid-state SERS substrates still rely on the expensive and sophisticated nanofabrication methods, such as FIB and EBL. From a practical perspective, the fabrication of efficient SERS substrates through large-area, low-cost and flexible methods, for instance, NSL, AAO and the SERS test papers, appears more suitable for practical applications. In this regard, we surveyed the recent progress of both emerging solid-state SERS substrates and their integration with microfluidic chips to foster their applications. Second, dynamic microfluidic trapping within SERS-enabled LoC devices was responsible for not only reliable SERS detection but also analyte manipulation. Accordingly, special attention should be paid to the manipulation accuracy, reduction of analyte loss and wide compatibility. Despite the lack of universal microfluidic trapping techniques for small molecules, successful examples in the case of DEP manipulations demonstrated great potential.

Although LoC systems intend to integrate all laboratory functions into a microfluidic chip, current SERS-enabled LoC systems still use bulky and costly instruments in laboratories. In the future, on-site analysis in the fields of health care, foods science and explosive detections requires portable microfluidic SERS detection systems. As palm-sized spectrometers for portable SERS detection have been on the market for a long period of time,

the next challenge for microfluidic SERS detection systems is the coupling of SERS-active chips with portable SERS spectrometers. A simple example will be to insert a nail-sized chip into a portable instrument for real-time analysis. With the rapid progress of microfluidics, lasers and spectrometers could also be integrated with microfluidic chips. Recent work with respect to the development of a microfluidic dye laser[141] may be a significant advancement. Overall, we expect hand-held microfluidic SERS detection systems to emerge in the market within years.

Received: ((will be filled in by the editorial staff))
Revised: ((will be filled in by the editorial staff))
Published online: ((will be filled in by the editorial staff))

References

1.   M. Shaban, A. G. A. Hady and M. Serry, *Ieee Sensors Journal*, 2014, **14**, 436-441.
2.   G. Wang, Z. Chen and L. Chen, *Progress in Chemistry*, 2010, **22**, 489-499.
3.   B. B. Xu, Y. L. Zhang, S. Wei, H. Ding and H. B. Sun, *Chemcatchem*, 2013, **5**, 2091-2099.
4.   P. N. Nge, C. I. Rogers and A. T. Woolley, *Chemical Reviews*, 2013, **113**, 2550-2583.
5.   D. Mark, S. Haeberle, G. Roth, F. von Stetten and R. Zengerle, *Chemical Society Reviews*, 2010, **39**, 1153-1182.
6.   S. Marre and K. F. Jensen, *Chemical Society Reviews*, 2010, **39**, 1183-1202.
7.   A. F. Chrimes, K. Khoshmanesh, P. R. Stoddart, A. Mitchell and K. Kalantar-zadeh, *Chemical Society Reviews*, 2013, **42**, 5880-5906.
8.   S. L. Kleinman, R. R. Frontiera, A. I. Henry, J. A. Dieringer and R. P. Van Duyne, *Physical Chemistry Chemical Physics*, 2013, **15**, 21-36.
9.   E. C. Le Ru, *Principles of surface-enhanced Raman spectroscopy and related plasmonic effects*, 1st ed. edn., Elsevier, Amsterdam ; Boston :, 2009.
10.   L. X. Chen and J. B. Choo, *Electrophoresis*, 2008, **29**, 1815-1828.
11.   M. Ringler, T. A. Klar, A. Schwemer, A. S. Susha, J. Stehr, G. Raschke, S. Funk, M. Borowski, A. Nichtl, K. Kurzinger, R. T. Phillips and J. Feldmann, *Nano Letters*, 2007, **7**, 2753-2757.
12.   J. R. Lombardi and R. L. Birke, *Accounts of Chemical Research*, 2009, **42**, 734-742.

13. K. B. Kim, J.-H. Han, H. Choi, H. C. Kim and T. D. Chung, *Small*, 2012, **8**, 378-383.
14. C. Lim, J. Hong, B. G. Chung, A. J. deMello and J. Choo, *Analyst*, 2010, **135**, 837-844.
15. H. Mao, W. Wu, D. She, G. Sun, P. Lv and J. Xu, *Small*, 2014, **10**, 127-134.
16. B. B. Xu, Y. L. Zhang, H. Xia, W. F. Dong, H. Ding and H. B. Sun, *Lab on a Chip*, 2013, **13**, 1677-1690.
17. H. Hwang and J.-K. Park, *Lab on a Chip*, 2011, **11**, 33-47.
18. M. R. Gartia, Z. Xu, E. Behymer, H. Nguyen, J. A. Britten, C. Larson, R. Miles, M. Bora, A. S. P. Chang, T. C. Bond and G. L. Liu, *Nanotechnology*, 2010, **21**, 395701.
19. E. Petryayeva and U. J. Krull, *Analytica Chimica Acta*, 2011, **706**, 8-24.
20. W.-H. Park and Z. H. Kim, *Nano Letters*, 2010, **10**, 4040-4048.
21. K. Uetsuki, P. Verma, T.-a. Yano, Y. Saito, T. Ichimura and S. Kawata, *Journal of Physical Chemistry C*, 2010, **114**, 7515-7520.
22. J. R. Lombardi and R. L. Birke, *Journal of Physical Chemistry C*, 2008, **112**, 5605-5617.
23. S. Maier, *Plasmonics: fundamentals and applications*, Springer, New York, 2007.
24. J. J. Baumberg, T. A. Kelf, Y. Sugawara, S. Cintra, M. E. Abdelsalam, P. N. Bartlett and A. E. Russell, *Nano Letters*, 2005, **5**, 2262-2267.
25. A. D. McFarland, M. A. Young, J. A. Dieringer and R. P. Van Duyne, *Journal of Physical Chemistry B*, 2005, **109**, 11279-11285.
26. B. Dong, L. Liu, H. Xu and M. Sun, *Journal of Raman Spectroscopy*, 2010, **41**, 719-720.
27. M. T. Sun, S. S. Liu, M. D. Chen and H. X. Xu, *Journal of Raman Spectroscopy*, 2009, **40**, 137-143.
28. M. Osawa, N. Matsuda, K. Yoshii and I. Uchida, *Journal of Physical Chemistry*, 1994, **98**, 12702-12707.
29. W. E. Smith, *Chemical Society Reviews*, 2008, **37**, 955-964.
30. J. A. Dougan and K. Faulds, *Analyst*, 2012, **137**, 545-554.
31. E. C. Le Ru, E. Blackie, M. Meyer and P. G. Etchegoin, *Journal of Physical Chemistry C*, 2007, **111**, 13794-13803.
32. R. Wilson, S. A. Bowden, J. Parnell and J. M. Cooper, *Analytical Chemistry*, 2010, **82**, 2119-2123.
33. M. J. Banholzer, J. E. Millstone, L. D. Qin and C. A. Mirkin, *Chemical Society Reviews*, 2008, **37**, 885-897.
34. I. M. White, S. H. Yazdi and W. W. Yu, *Microfluidics and Nanofluidics*, 2012, **13**, 205-216.
35. C. Delhaye, J.-L. Bruneel, D. Talaga, M. Guirardel, S. Lecomte and L. Servant, *Journal of Physical Chemistry C*, 2012, **116**, 5327-5332.
36. C. Andreou, M. R. Hoonejani, M. R. Barmi, M. Moskovits and C. D. Meinhart, *Acs Nano*, 2013, **7**, 7157-7164.
37. I. F. Cheng, C.-C. Lin, D.-Y. Lin and H. Chang, *Biomicrofluidics*, 2010, **4**, 034104.
38. P. C. Lee and D. Meisel, *Journal of Physical Chemistry*, 1982, **86**, 3391-3395.
39. P. G. Etchegoin and E. C. Le Ru, *Physical Chemistry Chemical Physics*, 2008, **10**, 6079-6089.
40. S. Lal, N. K. Grady, J. Kundu, C. S. Levin, J. B. Lassiter and N. J. Halas, *Chemical Society Reviews*, 2008, **37**, 898-911.
41. R. Huschka, A. Barhoumi, Q. Liu, J. A. Roth, L. Ji and N. J. Halas, *Acs Nano*, 2012, **6**, 7681-7691.
42. R. Bardhan, S. Lal, A. Joshi and N. J. Halas, *Accounts of Chemical Research*, 2011, **44**, 936-946.

43.   R. Huschka, J. Zuloaga, M. W. Knight, L. V. Brown, P. Nordlander and N. J. Halas, *Journal of the American Chemical Society*, 2011, **133**, 12247-12255.

44.   R. Huschka, O. Neumann, A. Barhoumi and N. J. Halas, *Nano Letters*, 2010, **10**, 4117-4122.

45.   H. Wang, D. W. Brandl, P. Nordlander and N. J. Halas, *Accounts of Chemical Research*, 2007, **40**, 53-62.

46.   A. Barhoumi, D. Zhang, F. Tam and N. J. Halas, *Journal of the American Chemical Society*, 2008, **130**, 5523-5529.

47.   J. Henzie, S. C. Andrews, X. Y. Ling, Z. Y. Li and P. D. Yang, *Proceedings of the National Academy of Sciences of the United States of America*, 2013, **110**, 6640-6645.

48.   M. J. Mulvihill, X. Y. Ling, J. Henzie and P. D. Yang, *Journal of the American Chemical Society*, 2010, **132**, 268-274.

49.   C. Hrelescu, T. K. Sau, A. L. Rogach, F. Jackel and J. Feldmann, *Applied Physics Letters*, 2009, **94,** 153113.

50.   H. Y. Liang, Z. P. Li, W. Z. Wang, Y. S. Wu and H. X. Xu, *Advanced Materials*, 2009, **21**, 4614-4618.

51.   J. F. Li, X. D. Tian, S. B. Li, J. R. Anema, Z. L. Yang, Y. Ding, Y. F. Wu, Y. M. Zeng, Q. Z. Chen, B. Ren, Z. L. Wang and Z. Q. Tian, *Nature Protocols*, 2013, **8**, 52-65.

52.   X. D. Tian, B. J. Liu, J. F. Li, Z. L. Yang, B. Ren and Z. Q. Tian, *Journal of Raman Spectroscopy*, 2013, **44**, 994-998.

53.   X. D. Lin, V. Uzayisenga, J. F. Li, P. P. Fang, D. Y. Wu, B. Ren and Z. Q. Tian, *Journal of Raman Spectroscopy*, 2012, **43**, 40-45.

54.   V. Uzayisenga, X. D. Lin, L. M. Li, J. R. Anema, Z. L. Yang, Y. F. Huang, H. X. Lin, S. B. Li, J. F. Li and Z. Q. Tian, *Langmuir*, 2012, **28**, 9140-9146.

55.   J. F. Li, J. R. Anema, Y. C. Yu, Z. L. Yang, Y. F. Huang, X. S. Zhou, B. Ren and Z. Q. Tian, *Chemical Communications*, 2011, **47**, 2023-2025.

56.   J. F. Li, S. Y. Ding, Z. L. Yang, M. L. Bai, J. R. Anema, X. Wang, A. Wang, D. Y. Wu, B. Ren, S. M. Hou, T. Wandlowski and Z. Q. Tian, *Journal of the American Chemical Society*, 2011, **133**, 15922-15925.

57.   J. F. Li, S. B. Li, J. R. Anema, Z. L. Yang, Y. F. Huang, Y. Ding, Y. F. Wu, X. S. Zhou, D. Y. Wu, B. Ren, Z. L. Wang and Z. Q. Tian, *Applied Spectroscopy*, 2011, **65**, 620-626.

58.   J. F. Li, Y. F. Huang, Y. Ding, Z. L. Yang, S. B. Li, X. S. Zhou, F. R. Fan, W. Zhang, Z. Y. Zhou, D. Y. Wu, B. Ren, Z. L. Wang and Z. Q. Tian, *Nature*, 2010, **464**, 392-395.

59.   J. Zhou, K. Ren, Y. Zhao, W. Dai and H. Wu, *Analytical and Bioanalytical Chemistry*, 2012, **402**, 1601-1609.

60.   H. Hwang, D. Han, Y. J. Oh, Y. K. Cho, K. H. Jeong and J. K. Park, *Lab on a Chip*, 2011, **11**, 2518-2525.

61.   M. J. Natan, *Faraday Discussions*, 2006, **132**, 321-328.

62.   D. X. Wang, W. Q. Zhu, M. D. Best, J. P. Camden and K. B. Crozier, *Nano Letters*, 2013, **13**, 2194-2198.

63.   C. D'Andrea, J. Bochterle, A. Toma, C. Huck, F. Neubrech, E. Messina, B. Fazio, O. M. Marago, E. Di Fabrizio, M. L. de la Chapelle, P. G. Gucciardi and A. Pucci, *Acs Nano*, 2013, **7**, 3522-3531.

64.   B. Sharma, R. R. Frontiera, A. I. Henry, E. Ringe and R. P. Van Duyne, *Materials Today*, 2012, **15**, 16-25.

65.   J. P. Camden, J. A. Dieringer, J. Zhao and R. P. Van Duyne, *Accounts of Chemical Research*, 2008, **41**, 1653-1661.

66.   K. A. Willets and R. P. Van Duyne, *Annual Review of Physical Chemistry*, 2007, **58**, 267-297.

67. E. C. Lin, J. Fang, S. C. Park, T. Stauden, J. Pezoldt and H. O. Jacobs, *Advanced Materials*, 2013, **25**, 3554-3559.

68. E. C. Lin, J. Fang, S. C. Park, F. W. Johnson and H. O. Jacobs, *Nature Communications*, 2013, **4,** 1636.

69. C. X. Wang, W. D. Ruan, N. Ji, W. Ji, S. Lv, C. Zhao and B. Zhao, *Journal of Physical Chemistry C*, 2010, **114**, 2886-2890.

70. S. K. Yang, W. P. Cai, L. C. Kong and Y. Lei, *Advanced Functional Materials*, 2010, **20**, 2527-2533.

71. T. Lohmuller, L. Iversen, M. Schmidt, C. Rhodes, H. L. Tu, W. C. Lin and J. T. Groves, *Nano Letters*, 2012, **12**, 1717-1721.

72. S. Mahajan, R. M. Cole, J. D. Speed, S. H. Pelfrey, A. E. Russell, P. N. Bartlett, S. M. Barnett and J. J. Baumberg, *Journal of Physical Chemistry C*, 2010, **114**, 7242-7250.

73. T. A. Kelf, Y. Sugawara, J. J. Baumberg, M. Abdelsalam and P. N. Bartlett, *Physical Review Letters*, 2005, **95,** 116802.

74. L. F. He, J. A. Huang, T. T. Xu, L. M. Chen, K. Zhang, S. T. Han, Y. He and S. T. Lee, *Journal of Materials Chemistry*, 2012, **22**, 1370-1374.

75. J. S. Shumaker-Parry, H. Rochholz and M. Kreiter, *Advanced Materials*, 2005, **17**, 2131.

76. H. Rochholz, N. Bocchio and M. Kreiter, *New Journal of Physics*, 2007, **9,** 53.

77. N. L. Bocchio, A. Unger, M. Alvarez and M. Kreiter, *Journal of Physical Chemistry C*, 2008, **112**, 14355-14359.

78. Y. Lu, G. L. Liu, J. Kim, Y. X. Mejia and L. P. Lee, *Nano Letters*, 2005, **5**, 119-124.

79. L. Y. Wu, B. M. Ross and L. P. Lee, *Nano Letters*, 2009, **9**, 1956-1961.

80. D. J. Lipomi, R. V. Martinez, M. A. Kats, S. H. Kang, P. Kim, J. Aizenberg, F. Capasso and G. M. Whitesides, *Nano Letters*, 2011, **11**, 632-636.

81. H. Im, N. J. Wittenberg, N. C. Lindquist and S. H. Oh, *Journal of Materials Research*, 2012, **27**, 663-671.

82. H. Im, K. C. Bantz, N. C. Lindquist, C. L. Haynes and S. H. Oh, *Nano Letters*, 2010, **10**, 2231-2236.

83. Y. Fang, N.-H. Seong and D. D. Dlott, *Science*, 2008, **321**, 388-392.

84. A. Kim, F. S. Ou, D. A. A. Ohlberg, M. Hu, R. S. Williams and Z. Y. Li, *Journal of the American Chemical Society*, 2011, **133**, 8234-8239.

85. F. S. Ou, M. Hu, I. Naumov, A. Kim, W. Wu, A. M. Bratkovsky, X. M. Li, R. S. Williams and Z. Y. Li, *Nano Letters*, 2011, **11**, 2538-2542.

86. M. Hu, F. S. Ou, W. Wu, I. Naumov, X. M. Li, A. M. Bratkovsky, R. S. Williams and Z. Y. Li, *Journal of the American Chemical Society*, 2010, **132**, 12820-12822.

87. M. S. Schmidt, J. Hubner and A. Boisen, *Advanced Materials*, 2012, **24**, OP11-OP18.

88. T. T. Xu, J. A. Huang, L. F. He, Y. He, S. Su and S. T. Lee, *Applied Physics Letters*, 2011, **99,** 153116.

89. Y. J. Oh and K. H. Jeong, *Advanced Materials*, 2012, **24**, 2234-2237.

90. Y. He, C. H. Fan and S. T. Lee, *Nano Today*, 2010, **5**, 282-295.

91. J. D. Caldwell, O. Glembocki, F. J. Bezares, N. D. Bassim, R. W. Rendell, M. Feygelson, M. Ukaegbu, R. Kasica, L. Shirey and C. Hosten, *Acs Nano*, 2011, **5**, 4046-4055.

92. Z. Y. Jiang, X. X. Jiang, S. Su, X. P. Wei, S. T. Lee and Y. He, *Applied Physics Letters*, 2012, **100,** 203104.

93. J. P. Coppe, Z. D. Xu, Y. Chen and G. L. Liu, *Nanotechnology*, 2011, **22**, 7, 245710.

94. Y. Wang, M. Becker, L. Wang, J. Liu, R. Scholz, J. Peng, U. Goesele, S. Christiansen, D. H. Kim and M. Steinhart, *Nano Letters*, 2009, **9**, 2384-2389.

95. H.-Y. Wu and B. T. Cunningham, *Applied Physics Letters*, 2011, **98,** 153103.

96. Y. D. Wang, N. Lu, W. T. Wang, L. X. Liu, L. Feng, Z. F. Zeng, H. B. Li, W. Q. Xu, Z. J. Wu, W. Hu, Y. Q. Lu and L. F. Chi, *Nano Research*, 2013, **6**, 159-166.

97. J. A. Huang, Y. Q. Zhao, X. J. Zhang, L. F. He, T. L. Wong, Y. S. Chui, W. J. Zhang and S. T. Lee, *Nano Letters*, 2013, **13**, 5039-5045.

98. Y. Zhao, J.-A. Huang, Z. Zhang, X. Chen and W. Zhang, *Journal of Materials Chemistry A*, 2014, **2**, 10218-10224.

99. R. Takahashi, T. Fukuoka, Y. Utsumi and A. Yamaguchi, *Japanese Journal of Applied Physics*, 2013, **52,** 06GK12.

100. J. Parisi, Y. Liu, L. Su and Y. Lei, *Rsc Advances*, 2013, **3**, 1388-1396.

101. J. Parisi, L. Su and Y. Lei, *Lab on a Chip*, 2013, **13**, 1501-1508.

102. J. Leem, H. W. Kang, S. H. Ko and H. J. Sung, *Nanoscale*, 2014, **6**, 2895-2901.

103. K. Herman, L. Szabo, L. F. Leopold, V. Chis and N. Leopold, *Analytical and Bioanalytical Chemistry*, 2011, **400**, 815-820.

104. B. B. Xu, R. Zhang, X. Q. Liu, H. Wang, Y. L. Zhang, H. B. Jiang, L. Wang, Z. C. Ma, J. F. Ku, F. S. Xiao and H. B. Sun, *Chemical Communications*, 2012, **48**, 1680-1682.

105. B. B. Xu, Z. C. Ma, H. Wang, X. Q. Liu, Y. L. Zhang, X. L. Zhang, R. Zhang, H. B. Jiang and H. B. Sun, *Electrophoresis*, 2011, **32**, 3378-3384.

106. B. B. Xu, Z. C. Ma, L. Wang, R. Zhang, L. G. Niu, Z. Yang, Y. L. Zhang, W. H. Zheng, B. Zhao, Y. Xu, Q. D. Chen, H. Xia and H. B. Sun, *Lab on a Chip*, 2011, **11**, 3347-3351.

107. Y. L. Zhang, Q. D. Chen, H. Xia and H. B. Sun, *Nano Today*, 2010, **5**, 435-448.

108. C.-h. Lai, L. Chen, G. Chen, Y. Xu and C.-y. Wang, *Applied Spectroscopy*, 2014, **68**, 124-127.

109. Y.-J. Oh and K.-H. Jeong, *Lab on a Chip*, 2014, **14**, 865-868.

110. B.-B. Xu, Z.-C. Ma, H. Wang, X.-Q. Liu, Y.-L. Zhang, X.-L. Zhang, R. Zhang, H.-B. Jiang and H.-B. Sun, *Electrophoresis*, 2011, **32**, 3378-3384.

111. V. Vlasko-Vlasov, A. Joshi-Imre, J. T. Bahns, L. Chen, L. Ocola and U. Welp, *Applied Physics Letters*, 2010, **96,** 203103.

112. Y. J. Oh, S. G. Park, M. H. Kang, J. H. Choi, Y. Nam and K. H. Jeong, *Small*, 2011, **7**, 184-188.

113. A. F. Chrimes, A. A. Kayani, K. Khoshmanesh, P. R. Stoddart, P. Mulvaney, A. Mitchell and K. Kalantar-zadeh, *Lab on a Chip*, 2011, **11**, 921-928.

114. Y.-L. Deng and Y.-J. Juang, *Biomicrofluidics*, 2013, **7,** 014111.

115. I. F. Cheng, H. C. Chang, T. Y. Chen, C. M. Hu and F. L. Yang, *Scientific Reports*, 2013, **3,** 2365.

116. V. Krivitsky, L.-C. Hsiung, A. Lichtenstein, B. Brudnik, R. Kantaev, R. Elnathan, A. Pevzner, A. Khatchtourints and F. Patolsky, *Nano Letters*, 2012, **12**, 4748-4756.

117. S. Yick, Z. J. Han and K. Ostrikov, *Chemical Communications*, 2013, **49**, 2861-2863.

118. I. Talian and J. Huebner, *Journal of Raman Spectroscopy*, 2013, **44**, 536-539.

119. G. Perozziello, R. Catalano, M. Francardi, E. Rondanina, F. Pardeo, F. De Angelis, N. Malara, P. Candeloro, G. Morrone and E. Di Fabrizio, *Microelectronic Engineering*, 2013, **111**, 314-319.

120. K. K. Strelau, T. Schuler, R. Moller, W. Fritzsche and J. Popp, *Chemphyschem*, 2010, **11**, 394-398.

121. N. Choi, K. Lee, D. W. Lim, E. K. Lee, S.-I. Chang, K. W. Oh and J. Choo, *Lab on a Chip*, 2012, **12**, 5160-5167.

122. E. Prado, A. Colin, L. Servant and S. Lecomte, *Journal of Physical Chemistry C*, 2014, **118**, 13965-13971.

123. A. Banerjee, R. Perez-Castillejos, D. Hahn, A. I. Smirnov and H. Grebel, *Chemical Physics Letters*, 2010, **489**, 121-126.

124. B. C. Galarreta, M. Tabatabaei, V. Guieu, E. Peyrin and F. Lagugne-Labarthet, *Analytical and Bioanalytical Chemistry*, 2013, **405**, 1613-1621.
125. H. Yun Suk and D. Erickson, *Biosensors & Bioelectronics*, 2010, **25**, 1240-1243.
126. F. Paquet-Mercier, N. B. Aznaveh, M. Safdar and J. Greener, *Sensors*, 2013, **13**, 14714-14727.
127. S. H. Yazdi and I. M. White, *Analytical Chemistry*, 2012, **84**, 7992-7998.
128. M. Fan, P. Wang, C. Escobedo, D. Sinton and A. G. Brolo, *Lab on a Chip*, 2012, **12**, 1554-1560.
129. F. L. Yap, P. Thoniyot, S. Krishnan and S. Krishnamoorthy, *Acs Nano*, 2012, **6**, 2056-2070.
130. A. Kim, S. J. Barcelo, R. S. Williams and Z. Y. Li, *Analytical Chemistry*, 2012, **84**, 9303-9309.
131. B. W. Li, W. Zhang, L. X. Chen and B. C. Lin, *Electrophoresis*, 2013, **34**, 2162-2168.
132. Y. H. Ngo, W. L. Then, W. Shen and G. Garnier, *Journal of Colloid and Interface Science*, 2013, **409**, 59-65.
133. L. L. Qu, Q. X. Song, Y. T. Li, M. P. Peng, D. W. Li, L. X. Chen, J. S. Fossey and Y. T. Long, *Analytica Chimica Acta*, 2013, **792**, 86-92.
134. W. W. Yu and I. M. White, *Analyst*, 2013, **138**, 3679-3686.
135. W. W. Yu and I. M. White, *Analytical Chemistry*, 2010, **82**, 9626-9630.
136. W. W. Yu and I. M. White, *Analyst*, 2013, **138**, 1020-1025.
137. Y. H. Ngo, D. Li, G. P. Simon and G. Garnier, *Langmuir*, 2012, **28**, 8782-8790.
138. R. Zhang, B. B. Xu, X. Q. Liu, Y. L. Zhang, Y. Xu, Q. D. Chen and H. B. Sun, *Chemical Communications*, 2012, **48**, 5913-5915.
139. C. H. Lee, M. E. Hankus, L. Tian, P. M. Pellegrino and S. Singamaneni, *Analytical Chemistry*, 2011, **83**, 8953-8958.
140. B. B. Xu, Y. L. Zhang, W. Y. Zhang, X. Q. Liu, J. N. Wang, X. L. Zhang, D. D. Zhang, H. B. Jiang, R. Zhang and H. B. Sun, *Advanced Optical Materials*, 2013, **1**, 56-60.
141. T. Wienhold, F. Breithaupt, C. Vannahme, M. B. Christiansen, W. Dorfler, A. Kristensen and T. Mappes, *Lab on a Chip*, 2012, **12**, 3734-3739.
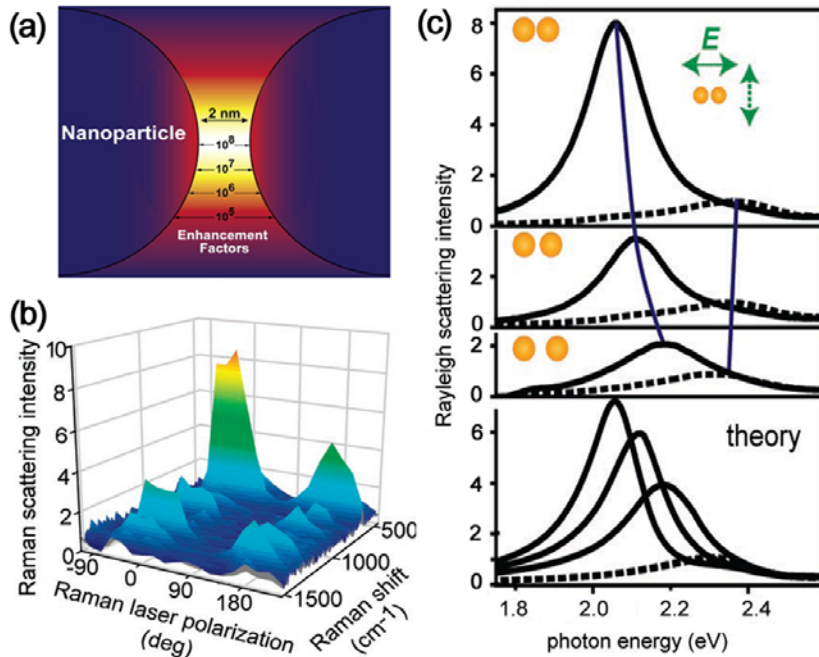
Figure 1. (a) An illustration of a hot spot for a nanoparticle dimer and rapid change in SERS EF with respect to nanogap spacing. Reproduced with permission19 (b) Typical polarization-dependent Raman spectra. Raman scattering is strong when the laser polarization is parallel to the dimer axis, leading to strong EME in the interparticle nanogaps and is weak for perpendicular polarization. (c) Experimental Rayleigh scattering enhancement from nanoparticle dimers at laser polarizations parallel (solid lines) and perpendicular (dashed lines) to the dimer axis, in comparison with calculated scattering cross sections (lowest panel). Both experiment and theory calculation indicated EME increased significantly with nanoparticle dimer axis parallel to laser polarization and the nanogap spacing less than 10 nm. Reproduced with permission.[11]
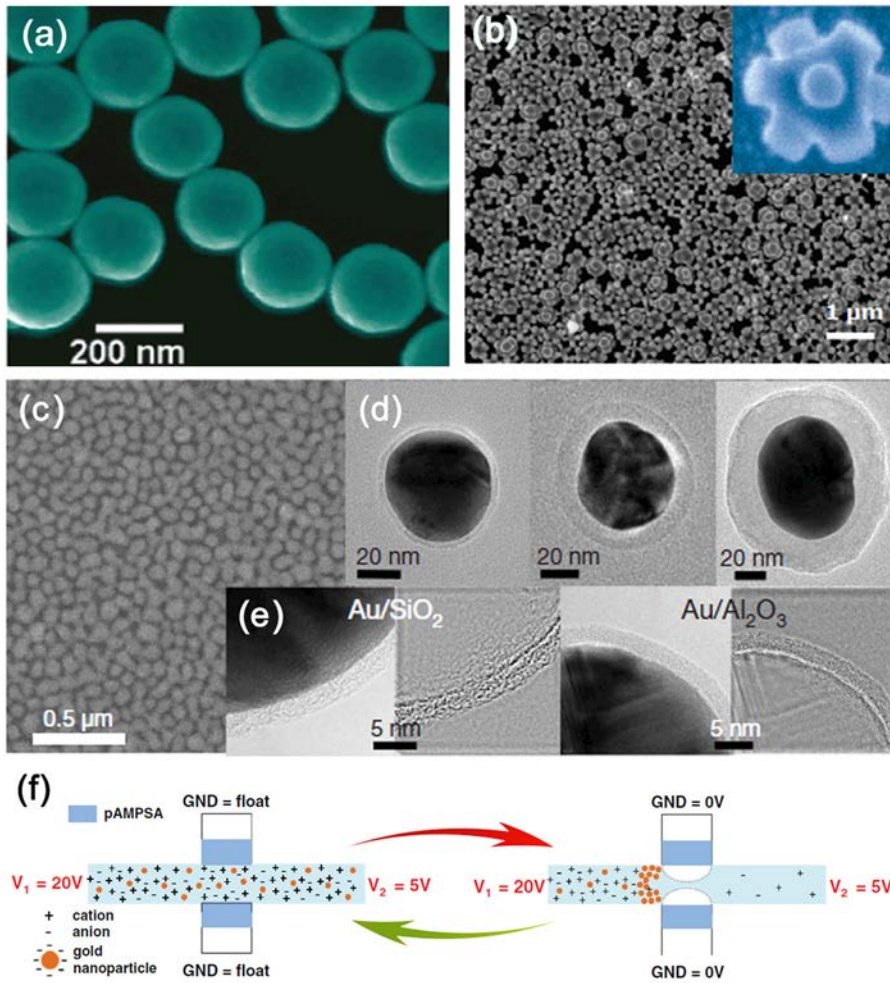
Figure 2. (a) SEM images of silica-Ag core-shell nanoparticles (nanoshells). Reproduced with permission[45] (b) SEM images of Ag octapod-shaped nanoparticles. Reproduced with permission[48] (c) SEM image of a monolayer of Au/SiO$_2$ nanoparticles on a smooth Au surface. (d) HRTEM images of Au/SiO$_2$ core–shell nanoparticles with different shell thicknesses. (e) HRTEM images of Au/SiO$_2$ nanoparticle and Au/Al$_2$O$_3$ nanoparticle. Reproduced with permission.[58] (f) Reversible pre-concetration mechanism with negatively charged polymer. Reproduced with permission[13]
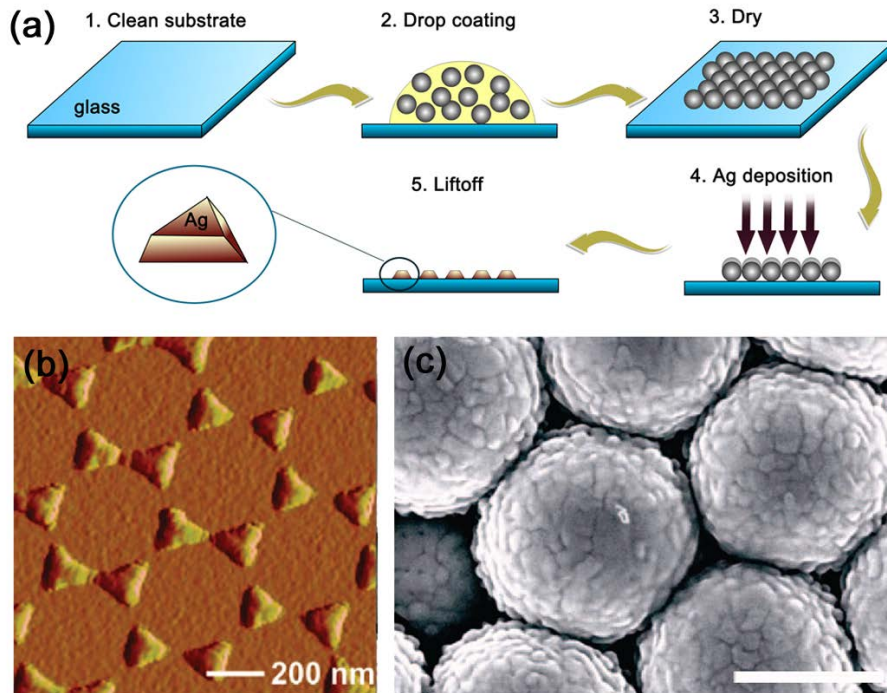
Figure 3. (a) Illustration of the process of NSL. Nanospheres are firstly drop-coated onto a clean substrate surface and allowed to self-assemble into a hexagonally close-packed array (steps 1–3), followed by Ag deposition to form AgFON (step 4), and removal of the nanospheres to make Ag nanotriangles (step 5). Reproduced with permission[66]; (b) AFM image of Ag nanotriangle array; (c) SEM image of AgFON. Reproduced with permission.[65]
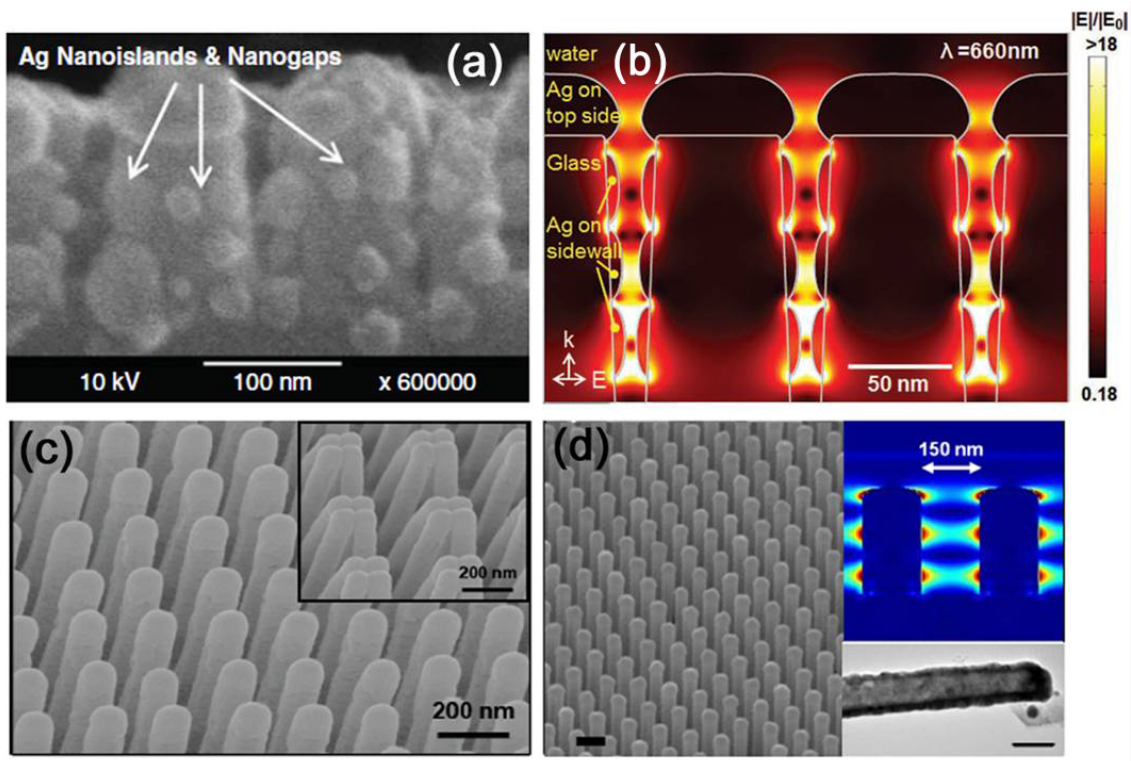
Figure 4. The SEM image (a) and the calculated electric field distribution (b) of high density hot spots generated by Ag nanoisland coated glass nanopillars; Reproduced with permission[89] (c) SEM images of freestanding nanofingers; inset: the closed nanofingers after molecule adsorption. Reproduced with permission[86] (d) SEM image of Ag/SiNW array; insets: simulated electric field intensity distribution of the 150 nm spaced Ag/SiNW array (upper) shows that the field is ~600 nm wide along the wire surface and a TEM image (lower) indicates the Ag layer is continuously formed on the silicon nanowire;. Reproduced with permission.[97]
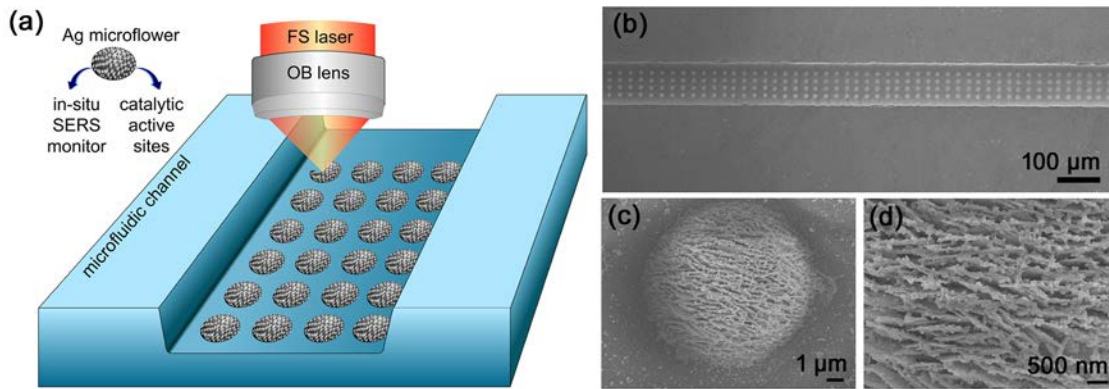
Figure 5. (a) Illustration of fabrication of Ag microflower as SERS substrates inside a microfluidic device by femtosecond laser direct writing induced photoreduction of Ag precursor. SEM images of the microflower-embedded microfluidic channel (b), microflower site (c) and the Ag nanostructure of the microflower (d). Reproduced with permission.[104]
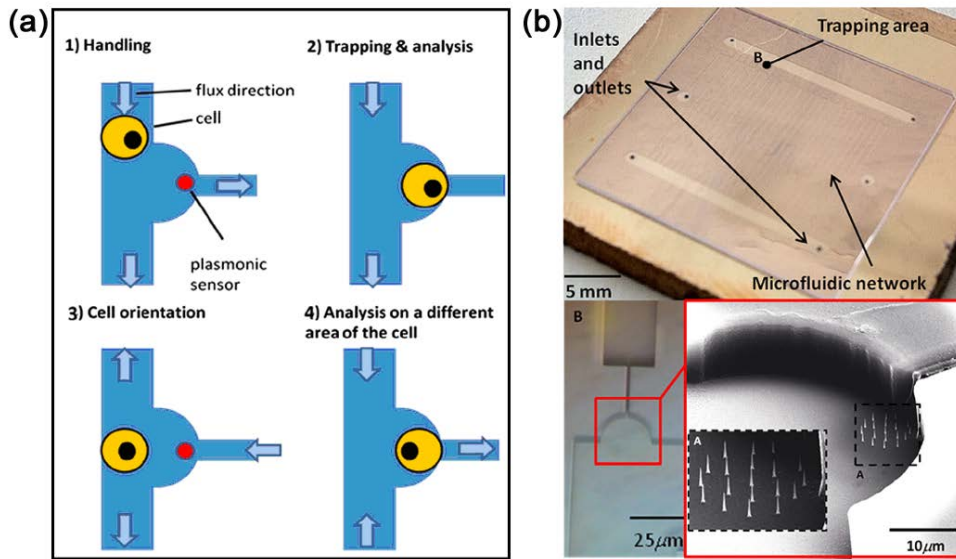
Figure 6. (a) schematic illustration of the cell trapping and analysis protocol. By changing the flow directions of the 3-way microfluidic channel, the cell could be directed to the plasmonic sensor site with different cell orientation such that different area of the cell wall could be analyzed by SERS technique. (b) bird view of the SERS microfluidic device (upper); optical image of the microfluidic trap (lower left); SEM image of the SERS-active microfluidic trap integrating the nanoneedls (lower right and inset) Reproduced with permission.[119]
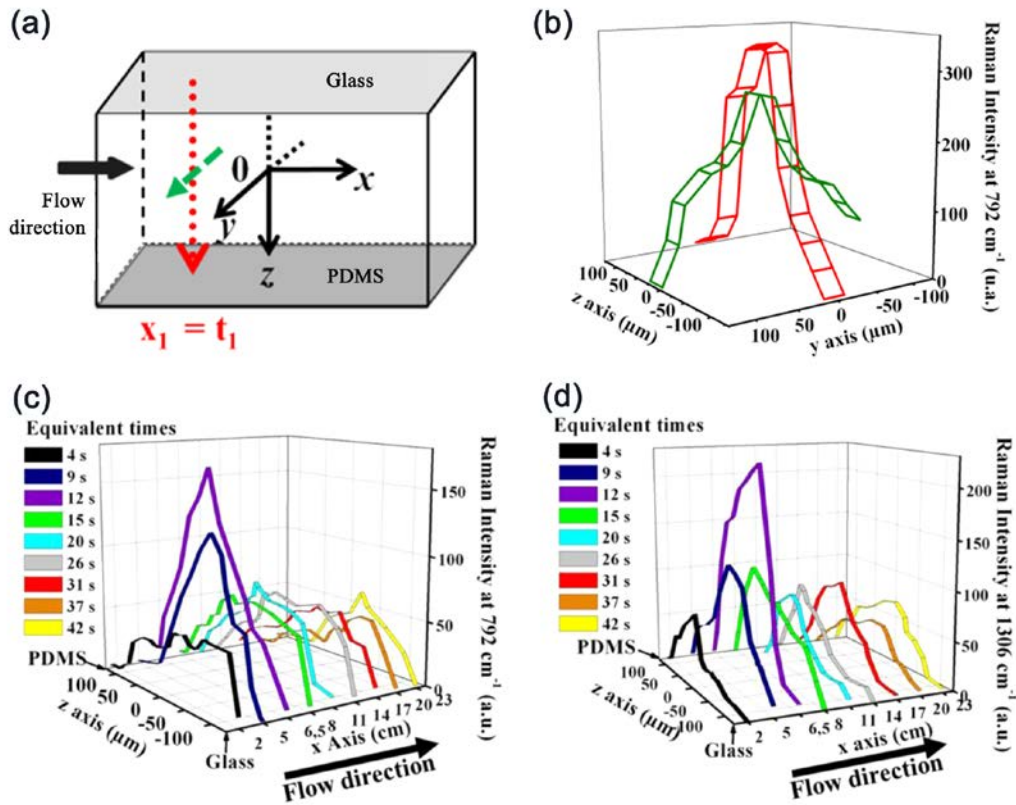
Figure 7. (a) Schematic illustration of a profile acquisition principle. The green and red arrows represent profile acquisitions along the y and z axis, respectively. (b) Profiles of 792 cm^{-1} band characteristic of polycytosine along the z and y axis for reaction times of 12 s. Profiles of bands characteristic of polycytosine (c) 792 cm^{-1} and (d) 1306 cm^{-1}, for different positions along the z axis, corresponding to various reaction times. Reproduced with permission.[122]
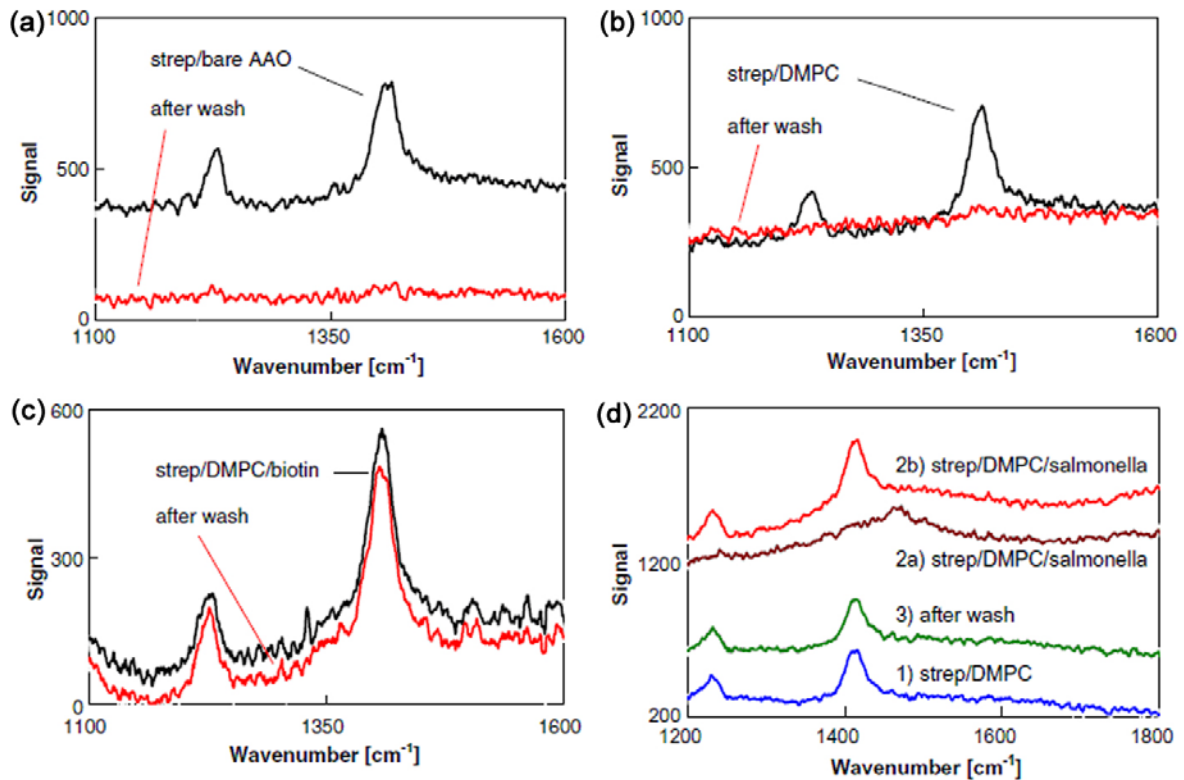
Figure 8. Raman spectra of streptavidin (strep) injected into microfluidic channel on (a) Bare AAO substrate and (b) AAO substrate impregnated with DMPC. The streptavidin could be easily washed away from either substrate as noted by the flat curves after wash. (c) Binding experiments: streptavidin attached to biotinylated DMPC before and after washing with water. (d) Sequenced experiments: 1) Raman spectra of streptavidin bound to biotinylated DMPC. 2a) The combined spectra when *S.enterica* was added to the channel. 2b) Spectra of streptavidin with *S. enterica* when the laser beam was focused onto the AAO surface of the channel. 3) After washing off the channel with water. Reproduced with permission.[123]
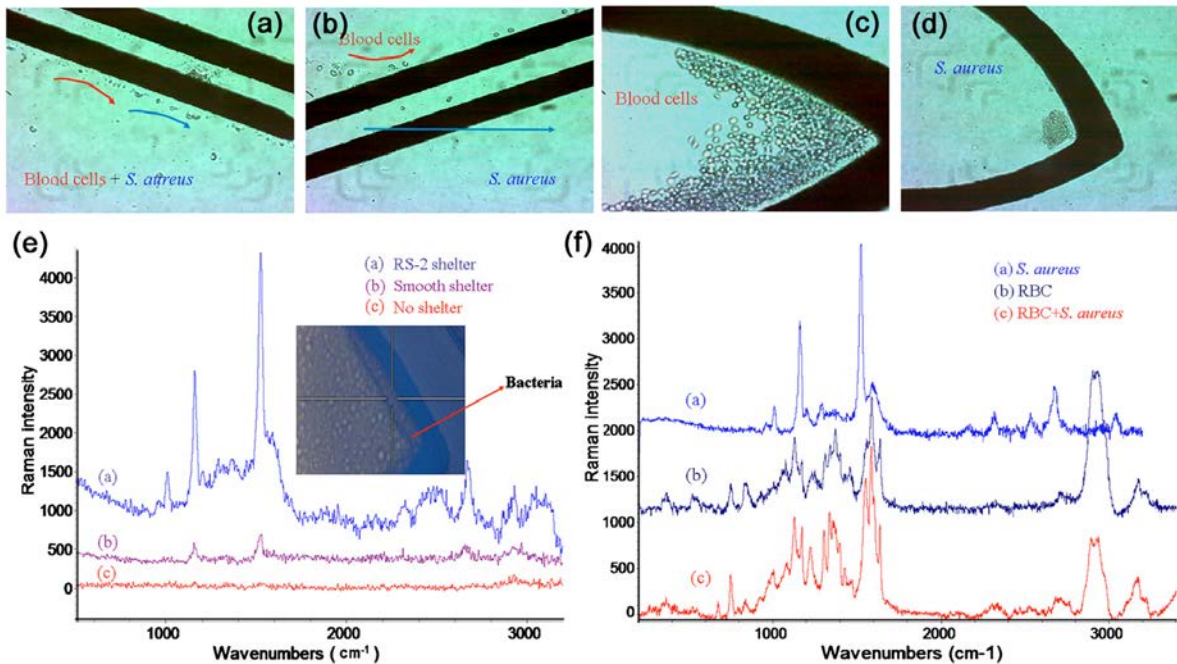
Figure 9. Experiment process of molecule guiding, sorting, and concentrating. (a) Blood cells and bacteria were guided to the sorting electrode by DEP and laminar flow. (b) Blood cells were repelled to the upper subchannel while bacteria penetrated the paired electrodeand flowed to the lower subchannel. Blood cells (c) and bacteria (d) were concentrated at their specific locations after the guiding and sorting steps. (e) The Raman spectra of *S. aureus* detected on the integrated chip after sorting from bacteria- red blood cell (RBC) mixture and concentrating into the detection location. Curves a, b, and c were obtained on a chip with a roughened Au shelter surface (RS-2), with smooth Au shelter, and without an Au shelter, respectively. The rough Au shelter surface exhibited the strongest SERS signals against fluorescence. (f) The SERS signatures of *S. aureus*, RBC, and RBCs/bacteria mixture. The detected SERS spectra of *S. aureus* and RBC after sorting and concentrating suggested that the RBC and bacteria were efficiently separated and detected on the chip. Reproduced with permission.[37]
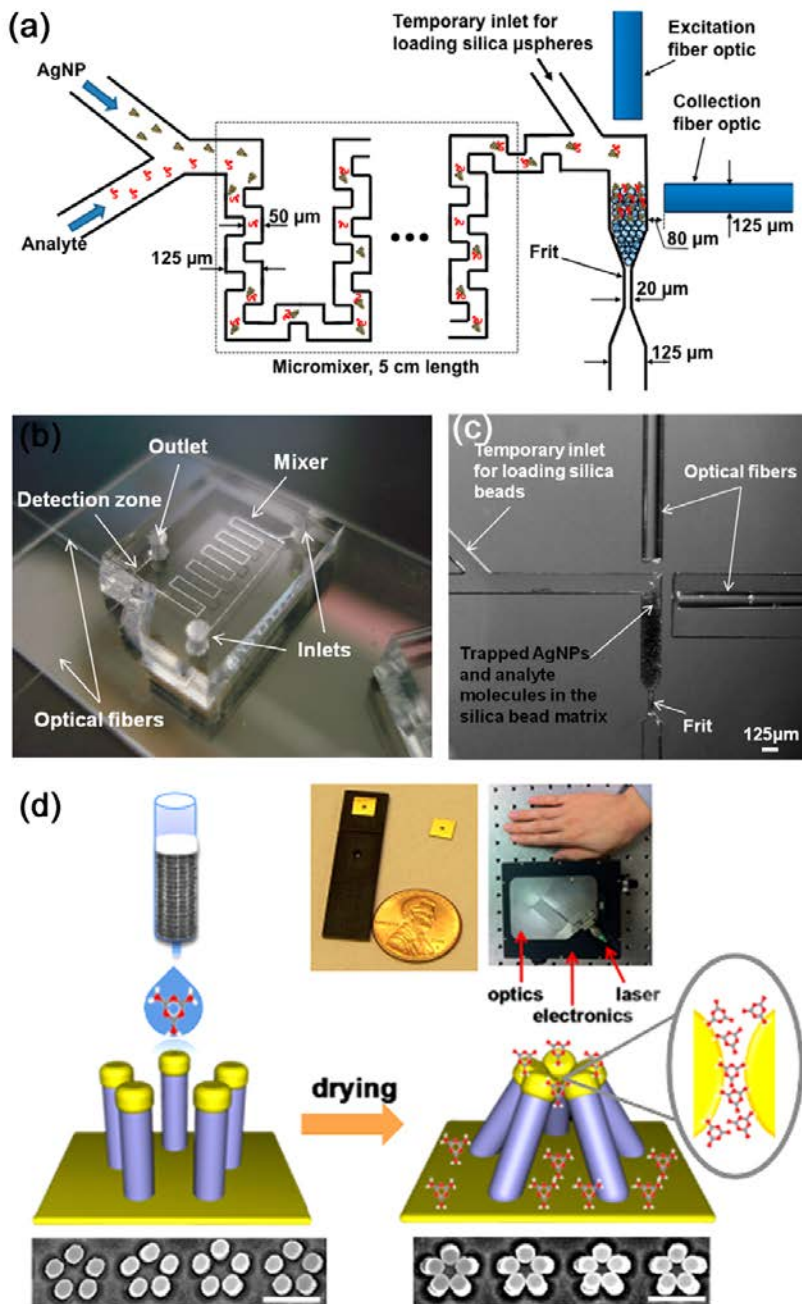
Figure 10. (a) Schematic of the SERS microfluidic system with fiber optic excitation and collection. (b) Photo of the SERS microfluidic system. (c) Microscope image of trapped microspheres and integrated fiber optic cables. Reproduced with permission[127] (d) Nanofinger-based SERS chip. The SEM images of open (left) and closed (right) gold nanofingers before and after drying of the filtered milk, respectively, are shown along with the illustration of how the gold nanofinger chips trapped the analyte molecules for molecular sensing. The photographs show the components of the prototype portable sensor system, which include the palm-sized portable spectrometer and the nanofingers chips, shown both unmounted and mounted on an aluminum strip. Reproduced with permission.[130]

Table 1. Fabrication methods, nanostructures and SERS performance of typical solid-state SERS substrates

Metal	Structures	Fabrication Methods	Max. EF	RSD [a] (%)	Number of spectra for calculating RSD	Reference
Ag	AgFON	NSL and RIE	10^5	6.5	30	69
Au	Nanovoids	NSL and Electrochemical Deposition	10^6	<10	80	24
Ag	AgNPs on nanopillar array	RIE and metal deposition	10^7	7.8	30	89
Ag	Aggregated Ag nanopillars	RIE and metal deposition	10^6	8	3000	87
Ag	Ag film on nanopillar array	NSL and wet etch	10^6	7	4624	97
Ag	Ag pyramid arrays	NSL and wet etch	10^7	8.8	20	96
Ag	AgNPs on silicon wafer	Reduction of silver citrate on silicon wafer	10^6	12.4	40	92
Ag	AgNPs on nanocone array	RIE and metal deposition	10^8	15.4	228	18

[a] RSD = (standard deviation)/mean, is relative standard deviation of the probed spectra.

Author Photograph(s)

Jian-An Huang received his BSc from University of Science and Technology of China in 2004. He joined the group of Prof. Shuit-Tong Lee in City University of Hong Kong in 2009 and obtained his PhD degree in Materials Science and Engineering in 2013. He is currently a Research Associate in the University of Hong Kong. His research interests include surface-enhanced Raman spectroscopy, scanning near-field optical microscopy, and metal/semiconductor plasmonic nanostructures.

Yong-Lai Zhang received his BS (2004) and PhD (2009) from Jilin University, China. He joined Jilin University in 2010 and is currently an associate professor in the State Key Laboratory on Integrated Optoelectronics, College of Electronic Science and Engineering, Jilin University. In 2011, he was awarded a "Hong Kong Scholar" postdoctoral fellow. His research interests include laser fabrication, and Lab-on-a-Chip system.

Hong-Bo Sun received his PhD from Jilin University, China, in 1996. He worked as a postdoctoral researcher in University of Tokushima, and an assistant professor in the Department of Applied Physics, Osaka University, respectively, from 1996 to 2005. In 2005, he became a professor (Changjiang Scholar) at Jilin University. His research has been focused on laser micro-nanofabrication, and their applications on microoptics, micromachines, microfluids, and microsensors.

With the rapid progress of microfluidics and optofluidics, surface enhanced Raman spectroscopy (SERS) has been successfully combined with Lab-on-a-Chip (LoC) systems for sensitive optofluidic dectection. In this review, we summarize the recent advances of SERS and microfluidics for development of reliable multifunctional SERS-enabled LoC systems and their broad chemical/biological applications.

Keyword: SERS; Lab-on-a-Chip (LoC) systems; microfluidics; Raman spectroscopy; optofluidic detection

Jian-An Huang, Yong-Lai Zhang,* Hong Ding, and Hong-Bo Sun*

SERS-enabled Lab-on-a-chip Systems